Journal of Materials and Environmental Science
ISSN : 2028-2508
e-ISSN : 2737-890X
CODEN : JMESCN

J. Mater. Environ. Sci., 2025, Volume 16, Issue 1, Page 163-178

http://www.jmaterenvironsci.com

Preparation and characterization of a photocatalyst based on clay impregnated with TiO_2

N'ZUE Yao Jean Vianney[1*], SORO Donafologo Baba[1], N'GUETTIA Kossonou Roland[1], YAYA Coulibaly [2], MEITE Ladji[1], TRAORE Karim Sory[1]**

[1]Laboratory of Environmental Sciences, UFR of Environmental Sciences and Management, NANGUI ABROGOUA University, 02 BP 801 Abidjan 02, Ivory Coast [2]Department of Chemical Engineering, Jilali University, P. M. B. 5025, [2]UFR-Agriculture, Fisheries Resources and Agro-industry, University of SAN-PEDRO, 01 BP 1800 SAN-PEDRO 01, Ivory Coast

** Corresponding author, Email address : njeanvianney@gmail.com*
*** Corresponding author, Email address : baba_soro@yahoo.fr*

Received *18 Dec 2024,*
Revised *21 Jan 2025,*
Accepted *23 Jan 2025*

Keywords:
- ✓ *Clay,*
- ✓ *Katiola,*
- ✓ *Titanium dioxide,*
- ✓ *Characterization,*
- ✓ *photocatalyst*

Citation*: N'zue Y. J. V., Soro D. B., N'guettia K. R., Yaya C., Meite L., Traore K. S. (2025) Preparation and characterization of a photocatalyst based on clay impregnated with TiO_2, J. Mater. Environ. Sci., 16(1), 163-178.*

Abstract: Titanium dioxide (TiO_2) is a widely used photocatalyst for eliminating pollutants from aqueous media. However, one of the drawbacks hindering its practical application is the difficulty in separating it from the reaction mixture, making it less reusable. This study aims to develop a material combining natural clay and TiO_2 with photocatalytic properties. The clay used comes from Katiola in the central northern Côte d'Ivoire. Beads were made from the ground clay fraction with a diameter between 45 and 125 µm. After calcination at 500 °C in a Nabertherm furnace, the beads were impregnated in a TiO_2 (anatase type) and recalcined at 400 °C for 2 h. The raw clay, calcined clay and clay-TiO_2 beads (photocatalyst) were characterized by X-ray diffraction (XRD), Fourier transform infrared spectroscopy (FTIR), scanning electron microscopy (SEM), energy dispersive X-ray spectroscopy (EDS), X-ray fluorescence (XRF) and BET (Brunauer Emmett Teller). The results of these analyses indicated that kaolinite was the main mineral component of this clay. These analyses also revealed a significant presence of TiO_2 in the clay-TiO_2 sample. BET analysis indicates that the specific surface area varies little with a larger pore volume and larger average pores in the clay-TiO_2 composite. This prepared photocatalyst appears to exhibit good photocatalytic properties under UV irradiation.

1. Introduction

Clay is one of the most widespread materials on the earth's surface and is available in many parts of the world (Ito and Wagai, 2017). This is the case, for example, in the Ivory Coast, where the Society for Mining Development (SODEMI) revealed the presence of numerous clay deposits dominated by kaolinites between 1964 and 1968 (Emeroua, 1993). The studies carried out on these materials highlight the importance of clay in different parts of the country. Indeed, because of its availability and abundance, it is used in many ways, particularly for craft activities (Touré and Kouassi, 2017; Abo *et al*., 2023). Today, faced with natural or man-made pollution of water resources, many researchers are more interested in eliminating identified pollutants using appropriate materials such as clay. Because of its mineralogical and physicochemical properties, clay is used as an adsorbent for environmental remediation, particularly in aqueous environments (N'guettia *et al*., 2019 ; Kedi *et al*., 2021 ; Soro *et*

al., 2023). In this context, its application sometimes requires improving its performance through the activation process (Djelloul *et al*., 2014). Even when activated, various problems arise during its use such as the processing time, which is fairly long. In some cases, it varies from 200 minutes to several hours (N'guettia *et al*., 2019 ; Soro *et al*., 2023), therefore a major concern. Furthermore, as the pollutant is not degraded, subsequent treatment is necessary, hence combining adsorption with a degradative process such as heterogeneous photocatalysis (Jaafar *et al*., 2019 ; Ainane *et al*., 2021; El Miz *et al*., 2024). Like clay, titanium dioxide used as a catalyst in the photocatalytic degradation process also presents serious problems, in particular, the economic loss in terms of catalyst recovery and recyclability for possible reuse. In addition, TiO_2 particles tend to aggregate, resulting in low adsorption capacity and low utilization of active sites (Shahid *et al*., 2015; Alshahateet *et al*., 2024; Abouri *et al*., 2024). However, one of the major challenges in this field concerns the reduction of treatment time and the degradation of refractory compounds (Dia *et al*., 2016; Zaaboul *et al*., 2024). Current treatment techniques involve a combination of chemical (photocatalysis) and physical (adsorption) methods (Fazal *et al*., 2020). The combination of these techniques involves fixing the TiO_2 on an adsorbent material, thus avoiding energy and time-intensive microfiltration at the end of the treatment process (Sraw *et al*., 2018). With this in mind, clays are receiving increasing attention as TiO_2 carriers because they are capable of adsorbing organic substances on their external surfaces as well as in their interlamellar spaces (Behilil *et al*., 2020 ; N'guettia *et al*., 2023). However, before considering using such materials, it seems necessary to know their properties.

This study aims to develop a material combining natural clay and TiO_2 with photocatalytic properties.

2. Materials and methods

2.1 Geographical location of the clay quarry

The clay used comes from Katiola, a commune located in the Hambol region in the centre- north of Côte d'Ivoire. Samples of clay material were taken at the respective coordinates (8°08'15" North latitude and 5°37'47" West longitude) and (8°08'22" North latitude; 5°37'41" West longitude) shown in **Figure 1**.

2.2 Sampling and pretreatment of clay material

The raw clay was taken from two potters' sites in the said commune. The samples were taken at different levels to ensure that they were representative. The samples sent to the laboratory were dried at room temperature, then crushed, sieved and placed in boxes for identification.

2.3 Preparation of the supported clay-TiO_2

The clay-TiO_2 supported photocatalyst material was prepared according to the following protocol: following pre-treatment, the clay fraction with a diameter between 45 and 125 µm was used to make clay beads. To do this, 50 mL of distilled water is added to 100 g of clay powder. The mixture is mixed by hand until the desired consistency and uniformity is achieved. The result is balls with a mass of between 0.25 and 0.28 g and a diameter of approximately 0.5 cm. They are dried in an oven at 60°C for 48 hours and then calcined in an oven at 500°C for 2 hours at a rate of 5°C/min. A TiO_2 suspension (anatase type) was then prepared by dissolving 10 g of TiO_2 powder in 500 mL of distilled water. The mixture is homogenised using a magnetic stirrer for 2 hours to obtain a good dispersion of the titanium particles. The clay beads prepared previously were soaked completely in the suspension and left there for 12 hours for complete adsorption of the catalyst. They were then dried in an oven at 100°C for 1

hour, then calcined at 400°C for 2 hours at a rate of 5°C/min. The beads were impregnated twice using the same process (Kaur *et al*., 2018). After washing with distilled water to remove the fraction of TiO_2 not adhered to the clay, they were dried at 100°C for 1 h and stored for use. **Figure 2** shows the steps involved in preparing the photocatalyst (clay-TiO_2).

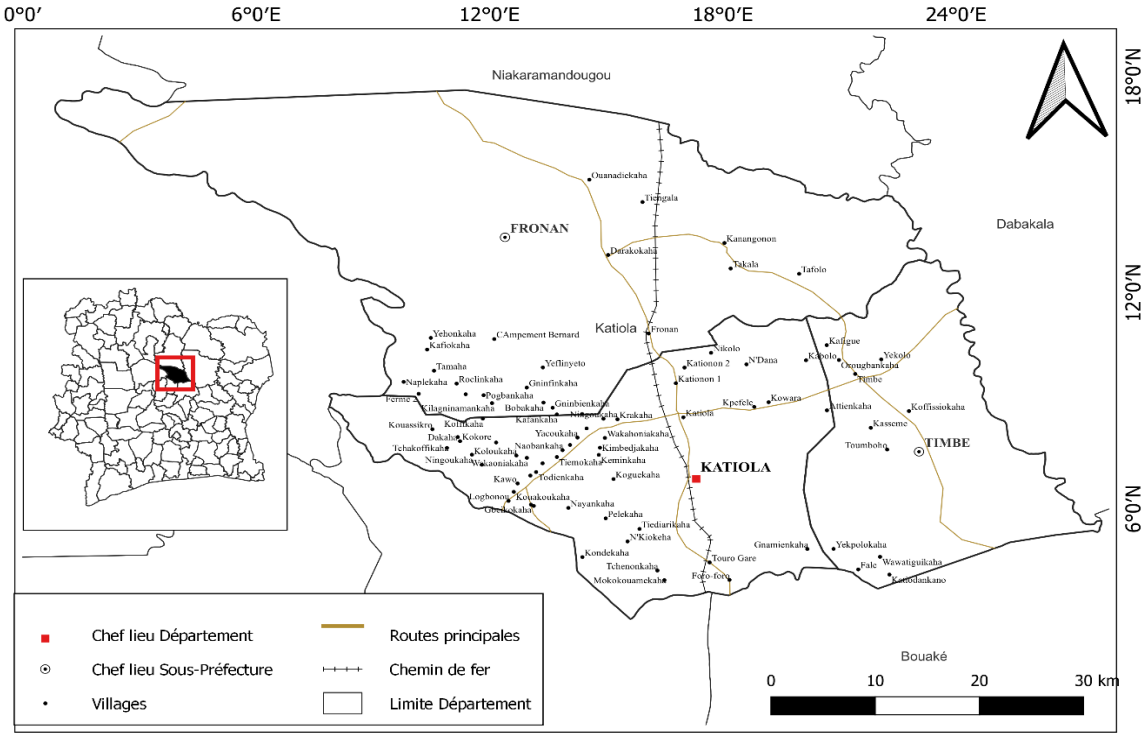

Figure1: Presentation of the study area

Figure 2: Preparation steps of the supported photocatalyst (clay-TiO_2)

2.3 Characterisation of calcined clay and the clay-TiO2

2.3.1 Humidity rate

Moisture content measurement is used to determine the mass of water eliminated by drying a moist material to a constant mass at a temperature of 105 ± 5°C for 24 hours. This parameter was determined on calcined and modified clay. A mass (m_1) of 1g of clay is weighed into a crucible. The whole is dried and then the mass (m_2) of the clay is determined. The moisture content is calculated using the following formula:

$$\boldsymbol{H(\%) = \frac{m_1 - m_2}{m_1} * 100} \qquad \textbf{(Eqn. 1)}$$

With :
H (%): moisture content in percent,
m1 (g): mass of clay at room temperature before drying,
m2 (g): mass of clay heated to 105°C for 24 hours.

2.3.2 Loss on ignition

The weight loss expressed as a percentage (%) is the weight loss of a sample after calcination at 1000°C, compared to the initial weight. It indicates the quantity of products likely to decompose or volatilise during firing. The loss on ignition was measured on calcined clay and modified by placing a quantity of 1 g of clay (mi) in a previously tared porcelain crucible. The assembly (crucible + clay) was then placed in a kiln, and the temperature was gradually increased to 1000°C for 2 hours, after which the mass mf was measured. The following relationship determines the value of the loss on ignition:

$$\boldsymbol{LOI}(\%) = \frac{\boldsymbol{m_i - m_f}}{\boldsymbol{m_i}} * \mathbf{100} \qquad \textbf{(Eqn.1)}$$

With :
mi: initial mass (g),
mf: final mass (g),
LOI: loss on ignition (%).

2.3.3 X-ray diffraction (XRD)

XRD analyses were carried out on all samples using a D8 ADVANCE (BRUKER AXS) equipped with a copper source and a LYNXEYE XE-T linear detector. This energy-discriminating detector eliminates the Kbeta line without using a nickel filter and attenuates the fluorescence phenomena influencing the signal-to-noise ratio. The angular range was in 2 θ between 3° and 65° for a step size of 0.024° and a step time of 1.5 seconds. The analyses therefore lasted approximately 1h 06 min. The support used was low background silicon to optimise the quality of the baseline. The diffractograms were processed using HighScore Plus software.

2.3.4 Fourier Transform Infrared (FTIR)

ATR (Total Attenuated Reflectance) spectra were carried out on all types of samples with a diamond tip, between wave numbers of 650 and 4000 cm^{-1} using a Nicolet iS50 FTIR spectrometer (ThermoFisher Scientific) and processed with OMNIC software. The spectra were taken without any preparation of the clay samples.

2.3.5 Scanning electron microscope (SEM)

A scanning electron microscope (SEM) coupled with energy dispersive analysis (EDS) was used to determine the qualitative chemical composition of the clay samples and observe their pore size and morphology. The EDS analysis was carried out using the Flat Quad detector at a voltage of 5 KV. The powder was deposited on a carbon lacquer, which acted as an adhesive and conductive film simultaneously. The samples were cleaned using the plasma Cleaner.

2.3.6 Elemental analysis by X-ray fluorescence spectrometry

Elemental analysis was carried out using a PANalytical - ZETIUM 2.4 kW X-ray fluorescence spectrometer (FRX). A quantity (g) of the sample was prepared into a bead to determine the chemical elements in the whole sample. It is then decanted into a dish to give it its final form, which is glass. The resulting glass is analysed by X-ray fluorescence.

2.3.7 Measurement of specific surface area by the Braunauer Emett and Teller (BET) method

Specific surface areas and pore volumes were measured using the TRISTAR 2, an instrument dedicated to the analysis of mesoporous samples by low-temperature nitrogen adsorption (77K). The clay samples

were degassed under vacuum at 90°C for 240 min, then immersed in liquid nitrogen to measure the specific surface area.

2.3.7 Point of zero charge (pH_{PZC})

The pH_{PZC} of raw, calcined and modified clay was determined by the pH method (Nwosu *et al*., 2018). This involves adding 0.1g of clay to vials containing 200 mL of 0.1 M NaCl solution, the initial pH of which is measured and adjusted from 1 to 12 using 0.1 M sodium hydroxide (NaOH) or hydrochloric acid (HCl) solutions. The bottles are closed and shaken for 24 hours, after which the final pH is measured. The difference between the initial pH (pHi) and final pH (pHf) values is plotted as a function of the initial pH (pHi). The point of intersection of the resulting curve with the x-axis gives the pHzpc value.

2.3.8 pH measurement

The pH of raw, calcined and modified clays is measured to determine the nature of their surface. The pH is determined by adding 100 mL of distilled water to a beaker containing 1g of powder of each type of clay. The solution was then stirred for 120 min and the pH measured.

3 Results and discussion

3.1 Physicochemical parameters

Table 1 shows the values of the various parameters relating to calcined clay and TiO_2 clay. The pH values of 6.5 and 6.7, respectively for calcined clay and TiO_2 clay reveal the acidic nature of these materials. This acidity is thought to be due to the mineral matter. The pH_{PZC} values for raw clay, calcined clay and clay-TiO_2 are 5.9, 4.2 and 5.5, respectively. Thus, the surface of the materials is positively charged for a pH < pH_{PZC} and negatively charged for a pH > pH_{PZC} (Adesina *et al*., 2023). This pH and pH_{PZC} values are very close to those obtained in previous studies indicating that Katiola clay is slightly acidic (Soro *et al*., 2011; Landi *et al*., 2019; He *et al*., 2023). Low moisture (H) levels are observed, which explains the non-hygroscopic nature of the materials. The loss on ignition (LOI) values for raw, calcined and clay-TiO_2 are 13.63%, 6% and 5% respectively. The low value (6.5%) would indicate the siliceous nature of this clay (Landi *et al*., 2019; He *et al*., 2023). The lower loss on ignition value obtained with clay6 TiO_2 would be linked to the double calcination, which would probably lead to greater mass loss in this material.

Table 1: Physicochemical parameters of materials

Raw clay				
Settings	**pH**	**pH_{PZC}**	**H (%)**	**LOI (%)**
Values	7.4	5.9	0.99	13.63
Calcined clay				
Settings	**pH**	**pH_{PZC}**	**H (%)**	**LOI (%)**
Values	6.5	4.2	0.5	6
Clay-TiO_2				
Settings	**pH**	**pH_{PZC}**	**H (%)**	**LOI (%)**
Values	6.7	5.5	1	5

*****LOI : Loss on ignition

3.2 X-ray diffraction (XRD)

Figures 3, 4 and **5** show the diffractograms obtained with raw clay, calcined clay and clay calcined with TiO_2. Examination of these diffractograms shows the presence of clay minerals and crystalline

phases. In **Figure 3** corresponding to the raw clay, peaks of medium intensity are observed. These are the peak at 2θ = 6.2° characteristic of smectite (Mache, 2013) and peaks at 2θ = 12.6°, 25° attributable to kaolinite (Maman *et al*., 2017). Low intensity peaks characteristic of kaolinite are also observed at 2θ = 20°, 35° (Cases, 1982 ; Boukhemkhem *et al*., 2017). Low intensity peaks observed at 2θ = 8.9°, 19°, 36°, 45.5° are attributable to micas (illites) (Zaki *et al*., 2008).

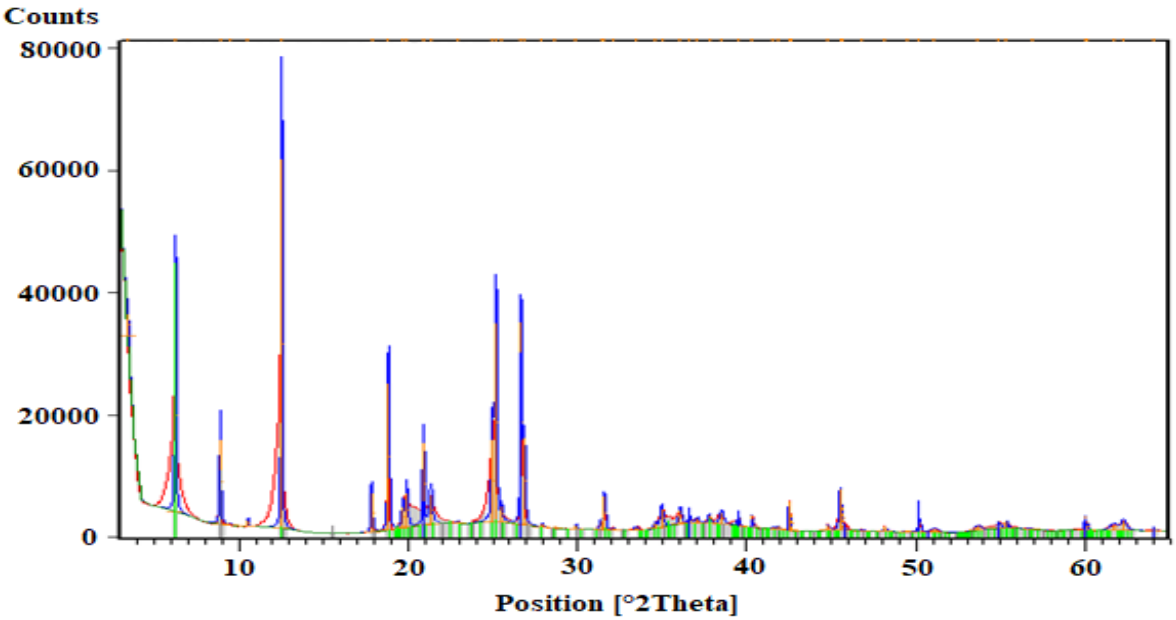

Figure 3: X-ray diffractogram of raw clay

Peaks identified at 2θ = 18°, 21°, 31.3°, 62.4° are similar to goethite. The presence of quartz is indicated by peaks at 2θ = 20.8°, 26.7°, 42.5°, 50° (Sei *et al*., 2004; Zaki *et al*., 2008). These results show that the clay used contains mainly kaolinite, which is associated with smectite, illite, goethite, and quartz as impurities. After calcination at 500°C of the clay samples with or without TiO2 (**Figures 4** and **5**), the diffractograms show the disappearance of peaks characteristic of kaolinite.

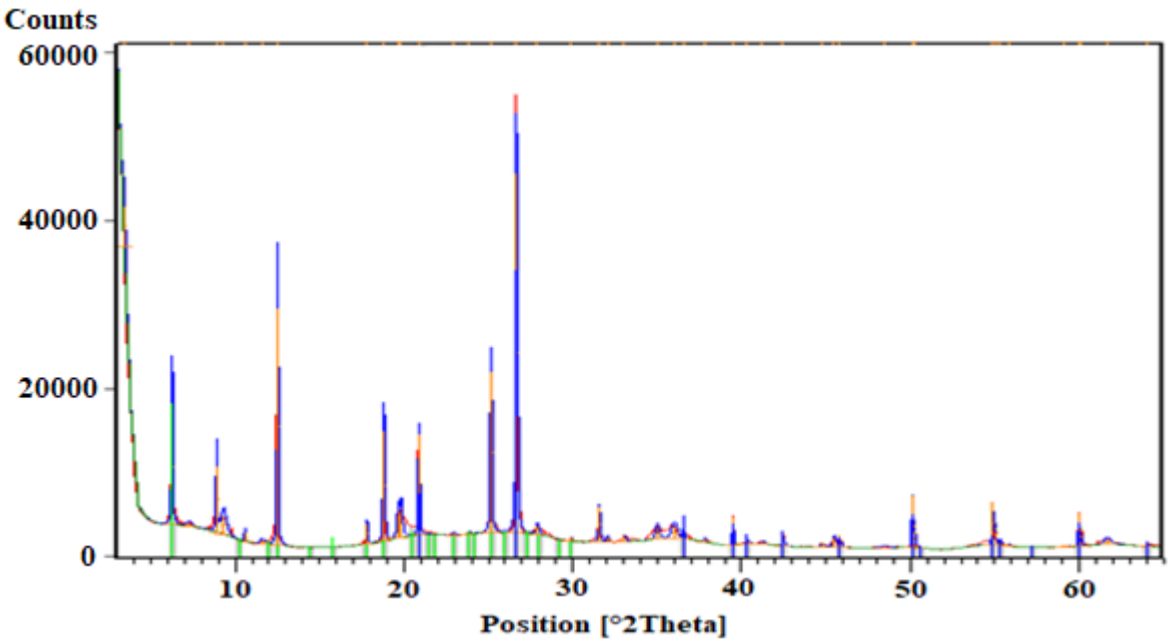

Figure 4: X-ray diffractogram of calcined clay

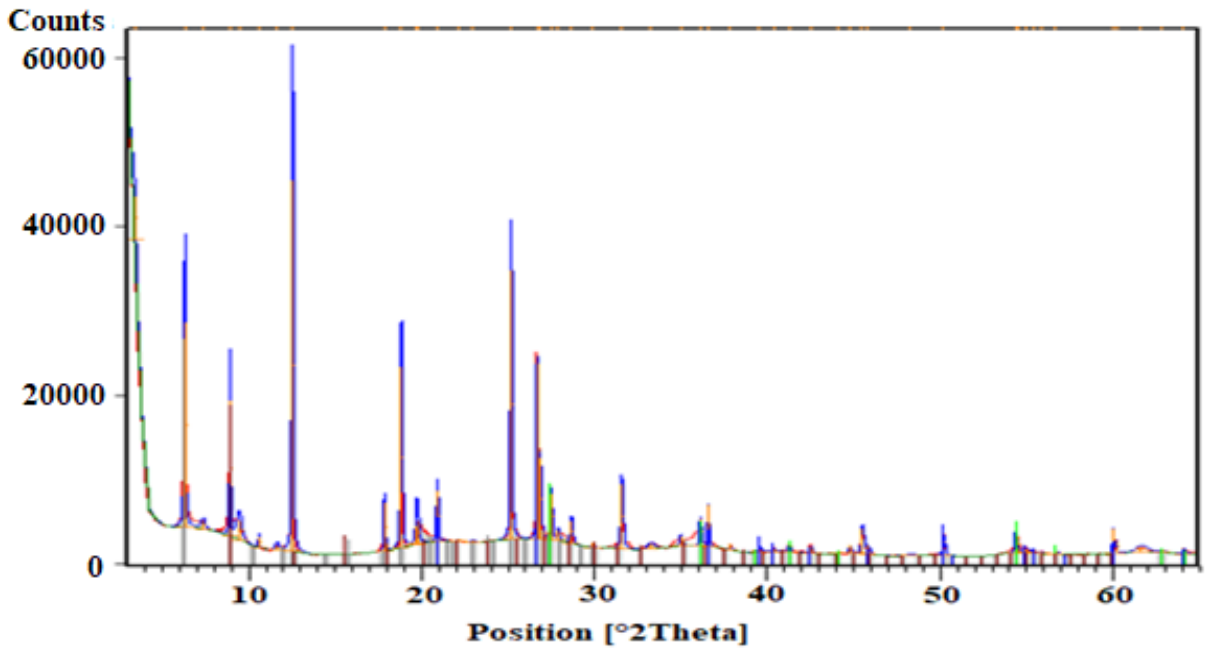

Figure 5: X-ray diffractogram of clay-TiO_2

In fact, studies have shown that dehydroxylation of kaolinite starts at a calcination temperature of 500°C causing alteration of its structure and leading to the formation of amorphous metakaolinite (Hollanders *et al*., 2016). There is also a decrease in the smectite and illite peaks. The spectrum of clay-TiO_2 shows the appearance of characteristic anatase TiO_2 peaks at values of 2θ = 25.5°, 36.5°, 37.5°, 46°, 55°, thus confirming the stability of the clay mineral following treatment at 500 °C.

3.3 Spectroscopy Fourier transform infrared (FTIR)

The FTIR spectra obtained for the three materials are shown in **Figure 6**. The spectra observed for calcined clay without and with TiO_2 are very similar, in contrast to that for raw clay. The broad absorption band observed for the raw clay sample between 3,200 and 3,700 cm^{-1} appears to be due to hydration. The absorption bands observed at 3682.2 cm^{-1} and 3619.9 cm^{-1} are characteristic of kaolinitic clay minerals. The peak at 3682.2 cm^{-1} is attributed to the elongation vibration (Al-OH) of the hydroxyl groups on the internal surface and the peak at 3619.9 cm^{-1} corresponds to the elongation vibration of the internal hydroxyl groups (Al-OH) (Madejova' and Komadel, 2001). The peak located at 1635 cm^{-1} is due to physisorbed water and is attributed to deformation (δ-OH) (Volzone et al., 2006; Hassan et al., 2011). The peak observed at 992.2 cm^{-1} indicates the presence of quartz and corresponds to Si-O elongation vibrations.

The band centred at 908.5 cm^{-1} corresponds to the vibrations of the Al-OH group present in kaolinite. The peak located at 790.5 cm^{-1} corresponds to the bending vibrations of the Si-O-Si quartz bond (Bouna *et al*., 2012) and also of the Fe-OH bond in goethite (Lakshmipathiraj *et al*., 2006). The absorption band observed at 748.7 cm^{-1} relates to Si-O-Al bonds (Aarfane *et al*., 2014). The IR spectra observed for the calcined samples (calcined clay and clay-TiO_2) are similar. The bands located around 3682 cm^{-1} and 3619 cm^{-1} disappeared under the effect of calcination, thus showing a disappearance of the kaolinite from these samples. The band's disappearance at 1635 cm^{-1} indicates the loss of the OH group of the free water. The dehydroxylation of the samples could explain this during calcination.

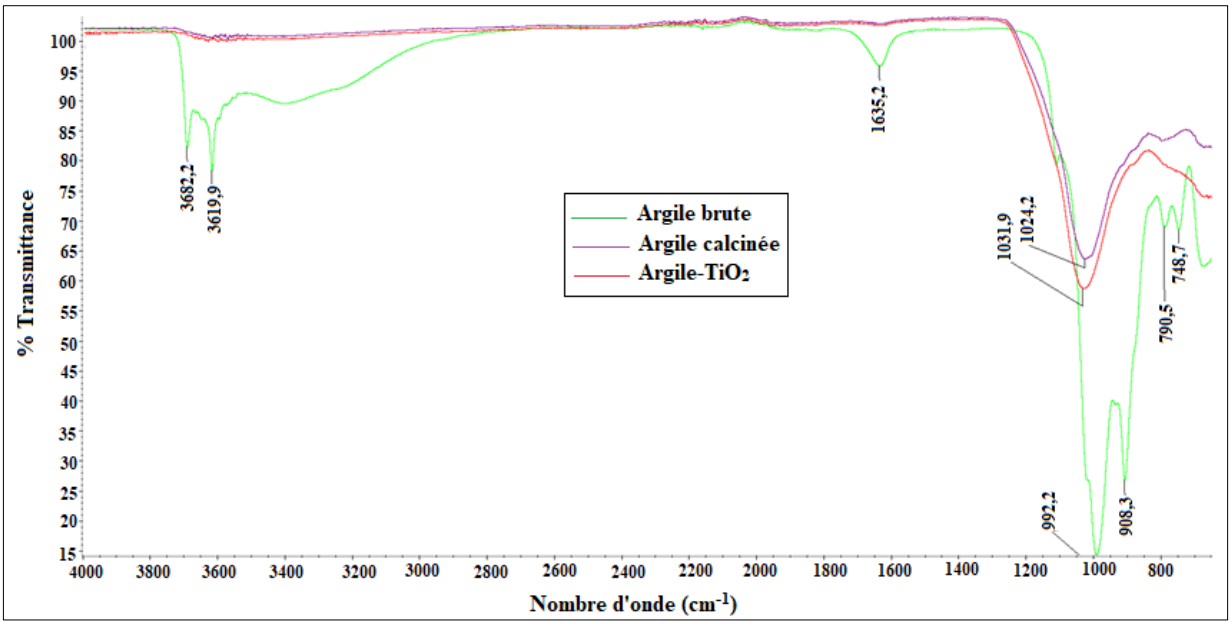

Figure 6: IR spectra of different samples

The bands located at 992 cm^{-1} and 908 cm^{-1}, originating from Si-O and Al-OH bonds respectively, also give way to less intense bands located at 1031.9 cm-1 and 1024.2 cm^{-1}, attributed respectively to the TiO_2 SiO_2 combination (Yang *et al*., 2013) and to the deformation vibrations of the Si-O-Si bonds of kaolinite or quartz. These spectra also reveal the disappearance of the bands at 790.5 cm^{-1} and 748.7 cm^{-1} reflecting the dehydroxylation of the clay. The results of the infrared spectra confirm the presence of minerals such as goethite, quartz and kaolinite, which were highlighted during the analysis of the X-ray diffractograms.

3.4 Scanning electron microscope (SEM)

SEM and EDS analyses were used to explore the microstructure and chemical composition of raw clay, calcined clay and clay-TiO_2 (**Figure 7**). The morphology of the raw clay (**Figure 7A**) has a well-defined book-like structure. Large aggregates of platelets with hexagonal contours and stacked on top of each other can be observed. According to Adamou *et al*. (2013), this structure is typical of a classic kaolinite. However, the stacking shows some defects, probably linked to the presence of other mineral structures such as quartz, which is observed in the image in the form of small grains. These results confirm the DRX and IR analyses indicating a significant amount of kaolinite in this clay. Similar results were obtained on clay samples from Côte d'Ivoire, showing that they were mainly composed of kaolinite (Konan *et al*., 2007; Konan *et al*., 2010; Gueu, 2019; Meite *et al*., 2021; Kouadio *et al*., 2022; Soro *et al*., 2023). The morphology of the calcined clay (**Figure 7B**) shows disordered structures with the absence of regular shapes, which would indicate a transformation of kaolinite into metakaolinite following heating at 500°C. Indeed, it has been shown that the dehydroxylation of kaolinite starts from a calcination temperature of 500 °C causing the alteration of its structure and leading to the formation of amorphous metakaolinite (Hollanders *et al*., 2016). The SEM image (**Figure 7C**) corresponding to the clay-TiO_2, shows a structure where the kaolinite appears to be completely transformed into metakaolinite due to repeated heating after impregnation of the clay in the TiO_2 solution. However, the presence of TiO_2 particles in the form of spheroidal grains is confirmed by chemical mapping (**Figure 7D**).

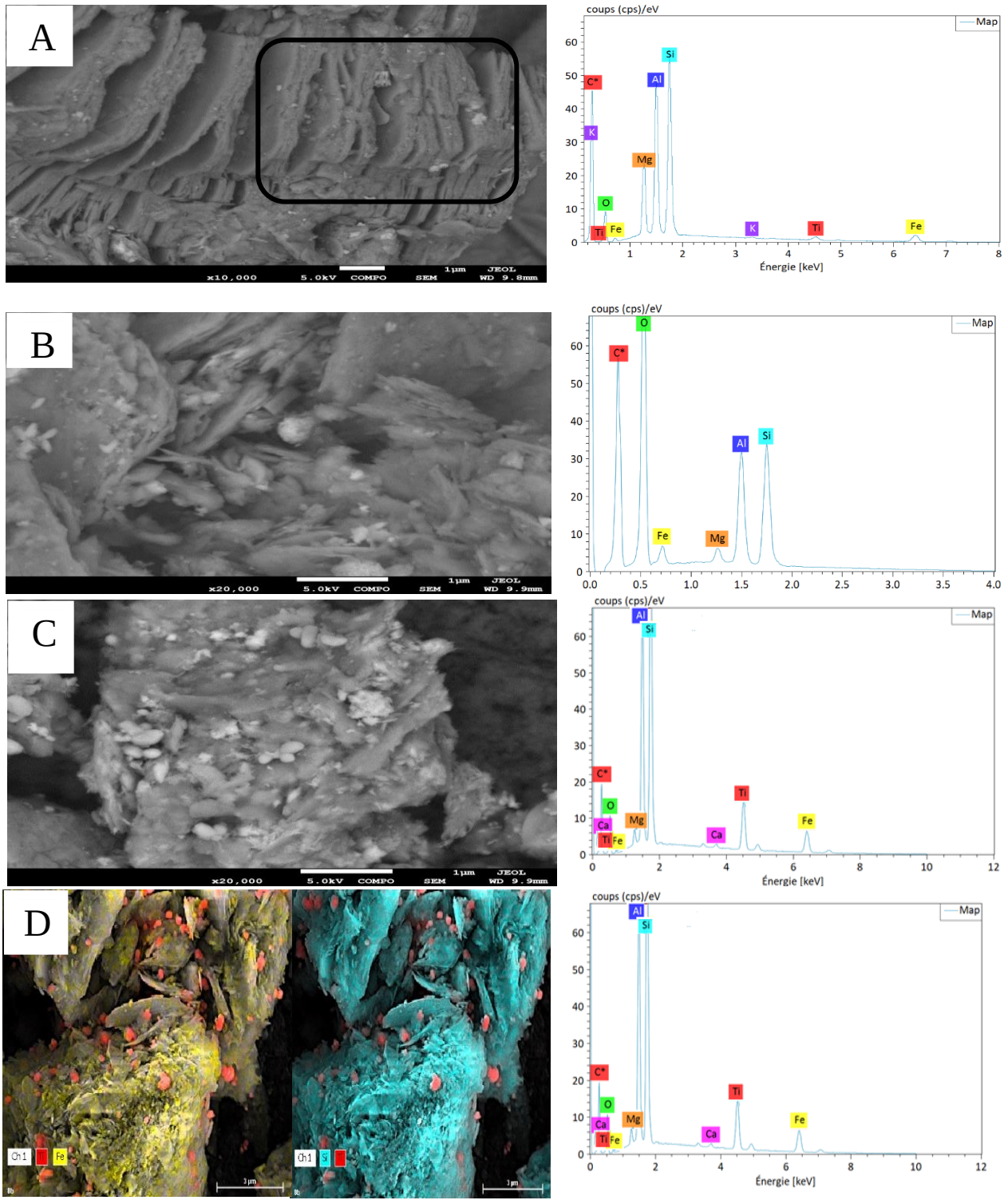

Figure 7: SEM micrographs and associated EDS spectra of raw clay (A), calcined clay (B) and clay-TiO_2 (C); Chemical mapping of clay-TiO_2 (D)

The associated EDS spectra indicate that all samples consist essentially of silicon (Si), aluminum (Al), iron (Fe), magnesium (Mg). In addition, the TiO_2 peak observed in the EDS spectrum of the raw clay appears very intense in that of the photocatalyst (clay-TiO_2), confirming the XRD results.

3.5 Elemental chemical analysis

The results of the XRF analysis of the samples are shown in **Table 2**.

Table 2: Chemical composition of materials (% by mass of oxide)

	SiO_2	Al_2O_3	Fe_2O_3	MgO	K_2O	TiO_2	CaO	Others	LOI	$\frac{SiO_2}{Al_2O_3}$	Total
Raw clay	49.40	29.60	16.20	2.33	0.94	0.63	0.51	0.39	13.63	1.67	100
Calcined clay	49.50	29.40	15.60	3.04	0.88	0.65	0.48	0.45	6.00	1.68	100
Clay-TiO_2	47.50	28.10	16.10	2.81	0.88	3.50	0.46	0.65	5.00	1.69	100

* LOI: Loss on ignition

According to this table, silica (SiO_2), alumina (Al_2O_3) and iron oxide (Fe_2O_3) are the major constituents of these samples. Silica and alumina being the predominant minerals indicate the silico-aluminous character of the clay used (Traoré, 2003 ; Eméruwa *et al*., 2008). The high proportion of silica (SiO_2) obtained can be attributed to the presence of a large quantity of quartz in this clay. Quartz is known for its high silica content and is commonly found as an impurity in clay material. The presence of iron oxide is consistent with the goethite peak on X-ray diffraction patterns. The high content of this oxide shows that Katiola clay is rich in iron, which is thought to be the reason for its yellow colour (Ségalen, 1969). Magnesium (Mg) is present in small quantities. The presence of K_2O and CaO (small quantities) indicates the existence of illite and smectite respectively in the Katiola clay. These results are in agreement with those reported by other authors concerning Katiola clay (Kouadio *et al*., 2022 ; He *et al*., 2023). All these elements, except TiO_2, have practically the same contents in both the raw and treated clay. There is an increase in the TiO_2 content in the impregnated clay (clay-TiO_2). This increase is thought to be due to the TiO_2 particles attached to the clay, thus indicating the success of the impregnation process (Said *et al*., 2023). The SiO_2/Al2O_3 mass ratio is around 1.67, indicating a high kaolinite content. However, this ratio is higher than the typical ratio of 1.18 found in kaolinites (Lecomte-Nana *et al*., 2013). This result can be explained by the possible presence of free quartz in significant proportions within the clay fraction (Gourouza *et al*., 2013). These results confirm those of XRD, IR and SEM.

3.6 Measurement of specific surface area using the BET method

Specific surface areas and pore volumes were measured on samples of raw clay, calcined clay and clay-TiO_2. The nitrogen adsorption/desorption isotherms at 77 K are shown in **Figure 8**. The curves shown in this figure show that these isotherms are type II according to the IUPAC classification. The presence of point B at these isotherms indicates that monolayer adsorption would occur before multilayer adsorption, and therefore that monolayer formation occurs followed by multilayer formation. The hysteresis loop, which does not end with a plateau at high p/p_0, shows that it is of type H_3. This type of hysteresis loop observed in the case where the adsorbent forms aggregates, can be attributed to capillary condensation which takes places in a non-rigid texture and is not characteristic of a defined mesoporosity.

It should also be noted that, whatever the type of sample (raw clay, calcined or impregnated in TiO_2), these isotherms show no difference, nor does the type of hysteresis. This means that the preparation methods adopted, after which these samples were calcined at 500°C and 400°C respectively for clay alone and clay-TiO_2, have no impact on the structural characteristics of the clay used.

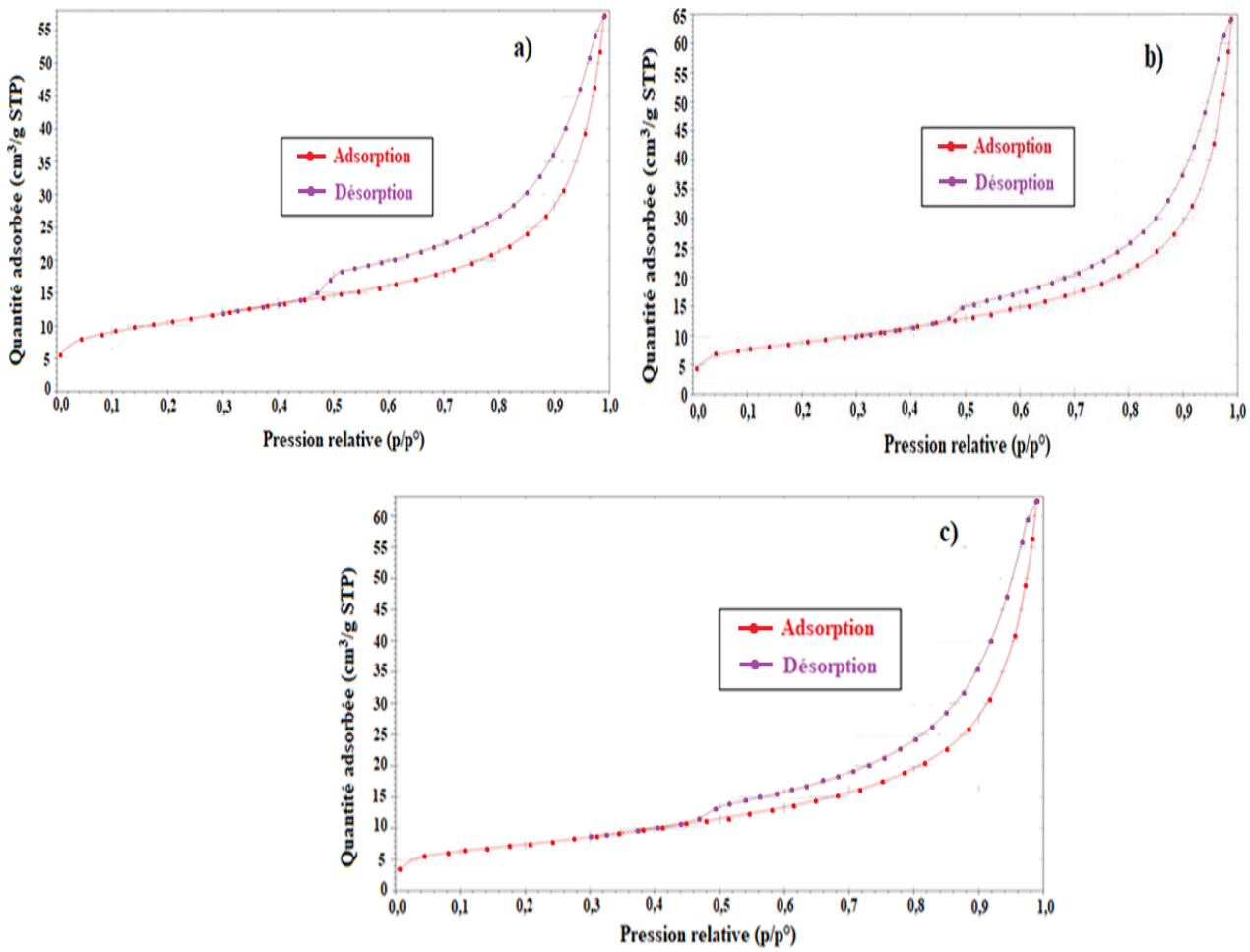

Figure 8: Adsorption and desorption isotherms for nitrogen at 77 K on clay, (a): raw clay; (b): calcined clay; (c): clay-TiO_2

Type II adsorption isotherms with H_3 hysteresis are typical of the materials used, as indicated by Rouquerol *et al*. (1999) and obtained by authors such as Wang *et al*. (2014), Deng *et al*. (2017) And Behilil *et al*. (2020). The structural characteristics of these materials are summarised in **Table 3**.

Table 3: Structural characteristics of raw, calcined and clay-TiO_2 samples

Samples	BET surface area ($m^2.g^{-1}$)	Pore volume (cm^3/g)	Volume microporous (cm^3/g)	Mesoporous volume (cm^3/g)	Average pore Å (ads 4V/A BET)
Raw clay	37.2	0.070	0.002	0.068	75
Calcined clay	31.4	0.078	0.002	0.076	100
Clay-TiO_2	28.6	0.075	0.000	0.075	112

BET analysis of raw, calcined and clays-TiO_2 shows that the specific surface area decreases from 37.2 to 28.6 $m^2.g^{-1}$ with an unchangeable microporous volume in raw and calcined clays, but none after impregnation with TiO_2. The pore and mesopore volumes are greater in calcined clay and clay- TiO_2. The mean pore volume values of these samples are 75, 100 and 112 Å for raw, calcined and impregnated clay respectively. The high pore volume and mesopore volume values for calcined clay are thought to be related to the calcination temperature. As this material is made up of three types of water, namely adsorbed, intercalary and structural water, their loss by desorption (evaporation) would

affect its porosity. At temperatures between 100 and 250°C, the clay loses adsorbed and intercalary water, followed by the loss of structural water at temperatures above 300°C. These results are similar to those obtained by Sun *et al* (2016) and Geng and Sun (2018). According to Sun *et al*. (2016), the oxidation and decomposition reaction of organic matter that occurs between 300 and 500°C could also influence the porosity of this material. The decrease in these pore volumes after the clay has been impregnated in the TiO_2 solution, would be attributed to the attached TiO_2 particles. According to Wang *et al*. (2014), the slight and abrupt increase leading to a stable adsorption state at low relative pressure isotherms ($p/p_0 < 0.1$) would indicate the existence of a small amount of micropores. This observation seems consistent with the results obtained due to the very low proportion of microporous volume available in raw clay and calcined clay. However, this microporous volume is non-existent in the TiO_2 clay, probably due to an obstruction of the pores by the TiO_2 particles. Like the pore and mesopore volumes, the calcination temperature also affects the specific surface area. The decrease in specific surface area initially (before impregnation) could be explained by the sintering process, which results in agglomeration of the clay particles under the effect of heat. These results are similar to those obtained by Dietel *et al* (2017) and Msinjili *et al*. (2019). We note that the value of the specific surface of the raw clay obtained is close to that obtained by Kedi *et al*. (2021). The reduction in specific surface area observed after impregnation can be explained by the attachment of TiO_2 particles to the surface of the clay, thus occupying certain active sites. In the same vein, Bel Hadjltaief *et al* (2015) indicate that the decrease in specific surface area and pore volume is linked to the presence of TiO_2 particles in the pores of the material. The increase in the average pore of these samples from 75 to 100 Å shows that there is pore creation within the clay due to calcination at 500°C. Then that from 100 to 112 Å would be attributed to pores created in the TiO_2 also under the effect of the calcination temperature. Similar observations were made by Mulewa *et al* (2017).

Conclusion

The clay-TiO_2 photocatalyst was successfully prepared by impregnating calcined clay beads in an anatase-type TiO_2 solution. This composite material and samples of raw and calcined clay were characterised by X-ray diffraction (XRD), Fourier transform infrared spectroscopy (FTIR), scanning electron microscopy (SEM) and EDS mapping analysis. The results of this characterisation identified kaolinite as the dominant component in the clay material. Also, all these analyses concur to clearly show nanometric particles of TiO_2 in the clay structure showing the stability of the clay mineral after treatment at 500°C. All the properties determined indicate that Katiola clay could produce a composite material (clay-TiO_2) with interesting photocatalytic activity. An experimental study using this photocatalyst to clean up contaminated water will be the subject of future work.

Acknowledgement, The technical inputs of Mr TRAORE Karim Sory and Mr SORO Donafologo Baba of Sciences Environment laboratory are acknowledged.

Disclosure statement: *Conflict of Interest*: The authors declare that there are no conflicts of interest.
Compliance with Ethical Standards: This article contains no studies involving human or animal subjects.

References

Aarfane A., Salhi A., El Krati M., S. Tahiri, Monkade M., Lhadi EK, Bensitel M. (2014), J. Mater. *Approximately. Sci.* 5 (6), 1928.

Abo, N., Koulaï, A., Tape, B.J. (2023). Ceramic Crafts in Katiola (Ivory Coast): A Historical-Cultural Activity at the Service of Female "Depauperization" in Rural Areas. *Journal of Research in Humanities and Social Science*, 11, pp: 110-117

Abouri, M., Benzaouak, A., Zaaboul, F., Sifou, A., Dahhou, M., et al. (2024). Efficient Catalytic Reduction of Organic Pollutants Using Nanostructured CuO/TiO_2 Catalysts: Synthesis, Characterization, and Reusability. *Inorganics*, *12*, 297. https://doi.org/10.3390/inorganics12110297

Adesina, M.O., Block, I., Günter, C., Unuabonah, EI, & Taubert, A. (2023). Efficient Removal of Tetracycline and Bisphenol A from Water with a New Hybrid Clay/TiO_2 Composite. *ACS Omega*, 8(24), 21594–21604. https://doi.org/10.1021/acsomega.3c00184

Ainane A., Taleb M., El-Hajjaji F., et al. (2021), Study of dependence between two types of most abundant natural clays in Bejaad province (Central Morocco) using a statistical approach, *Mor. J. Chem.* 9(2), 210-220, https://doi.org/10.48317/IMIST.PRSM/morjchem-v9i2.22438

Alshahateet S.F., Altarawneh R.M., Al-Tawarh W.M., et al. (2024), Catalytic green synthesis of Tin(IV) Oxide nanoparticles for phenolic compounds removal and molecular docking with EGFR Tyrosine Kinase *Scientific reports*, 14(1), 6519, https://doi.org/10.1038/s41598-024-55460-4

Behilil, A., Lahcene, D., Zahraoui, B., Benmehdi, H., & Belhachemi, M. (2020). Degradation of a cationic dye by solar photocatalysis through an Algerian clay impregnated with TiO2. *Algerian Journal of Environmental Science and Technology*, 6(4) pp 1566-1574

Bel Hadjltaief, H., Omri, A., Ben Zina, M., Da Costa, P., & Galvez, ME (2015). Titanium Dioxide Supported on Different Porous Materials as Photocatalyst for the Degradation of Methyl Green in Wastewaters. *Advances in Materials Science and Engineering*, 2015, 1-10. https://doi.org/10.1155/2015/759853

Boukhemkhem A., K. Rida (2017). Improvement adsorption capacity of methylene blue onto modified Tamazert kaolin. *Adsorption science and technology*, 35, 9-10, 753-773.

Bouna L., B. Rhouta, M. Amjoud, F. Maury, A. Jada, L. Daoudi, F. Senocq, M.-C. Lafont and C. Drouet (2012). Synthesis, characterizations and photocatalytic tests of a natural clay material based on TiO2-functionalized beidellite. *Materials & Techniques*, 100 (n°3). 241-252.

Cases, JM Lietard,O.Yvon,J. Delon, JF(1982). Study of the superficial morphological crystallochemical properties of disordered kaolinites. *Bull. Minéral*.105,439-455

Deng, L., Yuan, P., Liu, D., Annabi-Bergaya, F., Zhou, J., Chen, F., & Liu, Z. (2017). Effects of microstructure of clay minerals, montmorillonite, kaolinite and halloysite, on their benzene adsorption behaviors. *Applied Clay Science*, 143, 184–191. https://doi.org/10.1016/j.clay.2017.03.035

Dia, O., Drogui, P., Dubé, R., & Buelna, G. (2016). Use of electrochemical processes and their combinations with biological processes for the treatment of leachates from sanitary landfills—Literature review. *Water Science Review*, 29(1), 63-89. https://doi.org/10.7202/1035717ar

Dietel, J., Warr, L.N., Bertmer, M., Steudel, A., Grathoff, G.H., & Emmerich, K. (2017). The importance of specific surface area in the geopolymerization of heated illicit clay. *Applied Clay Science*, 139, 99-107. https://doi.org/10.1016/j.clay.2017.01.001

Djelloul, B., Driss, A., & Djillali, B. (2014). Adsorption of copper Cu (II) in solution by raw and activated clay from the Tiout-Naama region, southwest Algeria. *Materials Science Review*, No. 2 pp.23-34 http://archives.univ-biskra.dz/handle/123456789/3812

El Miz M., Loutou M., Aaddouz M., Tahani A., et al. (2024) Thermal release of Thymol encapsulated into sodium, organic and pillared modified clay matrixes, *Chemical Papers*, 78, 1585–1599, https://doi.org/10.1007/s11696-023-03186-4

Emeroua, E. (1993). Raw materials for ceramic use in Ivory Coast. Assessment and prospects. SODEMI Report, 634, 4-16.

Emeruwa, E., Kouadio, KC, Kouakou, CH, Boffoue, OM, Assande, AA, Ouattara, S., Coulibaly, Y., Dauscher, A., & Lenoir, B. (2008). Characterization of clays in the Abidjan region: Comparative study of some deposits and their development prospects. *Revue.Ivoirienne. Sciences. Technologie*, 11, 177–192

Fazal, T., Razzaq, A., Javed, F., Hafeez, A., Rashid, N., Amjad, US, Rehman, MSU, Faisal, A., & Rehman, F. (2020). Integrating adsorption and photocatalysis: A cost effective strategy for textile wastewater treatment using hybrid biochar-TiO2 composite. *Journal of hazardous materials*, 390, 121623.

Geng, J., & Sun, Q. (2018). Effects of high temperature treatment on physical-thermal properties of clay. *Thermochimica Acta*, 666, 148-155. https://doi.org/10.1016/j.tca.2018.06.018

Gourouza M., A. Zanguina, I. Natatou, and B. Anne (2013). Characterization of a mixed clay from Niger. *Rev. CAMES-Sci. Struct. Mat*., Vol. 1, 29-39.

Gueu Soumahoro (2019) Elimination of Humic Acids Present in Water by Adsorption and/or Photocatalysis. Doctoral Thesis, National Polytechnic Institute Houphouët Boigny (INPHB), Yamoussoukro, Ivory Coast, 121p.

Hassan H., BH Hameed (2011). Fe-clay as effective heterogeneous catalyst for the decolorization of Reactive blue 4. *Chemical Engineering Journal*, 171, 912–918.

He, IL, Atheba, GP, Allou, NB, Drogui, P., Khakani, MAE, & Gbassi, GK (2023). Physic, Chemical and Mineralogical Characterizations of Clays Used in the Making of Traditional Ceramics in the City of Katiola, Ivory Coast. *Journal of Minerals and Materials Characterization and Engineering*, 11(04), 81-91. https://doi.org/10.4236/jmmce.2023.114008

Hollanders S., R. Adriaens, J. Skibsted, Ö. Cizer, and J. Elsen (2016). Pozzolanic reactivity of pure calcined clays. *Appl. Clay Sci*., 133, 1–9

Ito, A., & Wagai, R. (2017). Global distribution of clay-size minerals on land surface for biogeochemical and climatological studies. *Scientific Data*, 4(1), 170103. https://doi.org/10.1038/sdata.2017.103

Jaafar A, HB El Ayouchia, Z Lakbaibi, A Boussaoud, S Jodeh, K Azzaoui,et al. (2019) GP Globalize Research Journal of Chemistry, Degradation of pollutant dye in aqueous solution using Fenton reaction: a DFT study, *Desalination and Water Treatment*, 158, 364–371, https://doi.org/10.5004/dwt.2019.24261

Karfa Traoré (2003). Low-temperature sintering of a kaolinitic clay from Burkina Faso. Thermal transformations and structural reorganizations. Doctoral thesis, University of Limoges, France, 209 p.

Kaur, T., Sraw, A., Wanchoo, R.K., & Toor, A.P. (2018). Solar assisted degradation of carbendazim in water using clay beads immobilized with TiO_2 & Fe doped TiO_2. *Solar Energy*, 162, 45-56.

Kedi, ABB, Kouassi, SS, Coulibaly, V., & Sei, J. (2021). Elimination of pollutants from liquid waste of a sugar production unit by natural clays from Côte d'Ivoire. *International Journal of Biological and Chemical Sciences*, 15(2), 803-815.

Konan, KL, Peyratout, C., Bonnet, J.-P., Smith, A., Jacquet A., Magnoux, P. & Ayrault, P. (2007). Surface properties of kaolin and illite suspensions in concentrated calcium hydroxide medium. *Journal of Colloid and Interface Science*, 307(1), 101-108

Konan, L.K., Soro, J., Andji, J.Y.Y., Oyetola, S. and Kra, G. (2010). Comparative Study of Dehydroxylation/Amorphization in Two Kaolins of Different Crystallinity. *Journal of the West African Chemical Society*, 30, 29-39.

Kouadio, LM, Lebouachera, SEI, Blanc, S., Sei, J., Miqueu, C., Pannier, F., & Martinez, H. (2022). Characterization of Clay Materials from Ivory Coast for Their Use as Adsorbents for Wastewater Treatment. *Journal of Minerals and Materials Characterization and Engineering*, 10(04), 319-337. https://doi.org/10.4236/jmmce.2022.104023

Lakshmipathiraj P, Narasimhan BRV, Prabhakar S, Raju GB (2006). Adsorption of arsenate on synthetic goethite from aqueous solutions, *J. Hazard. Mater*, (136), 281 – 287.

Landi, S., Carneiro, J., Soares, OSGP, Pereira, MFR, Gomes, AC, Ribeiro, A., Fonseca, AM, Parpot, P., & Neves, IC (2019). Photocatalytic performance of N-doped TiO2nano-SiO2-HY nanocomposites

immobilized over cotton fabrics. *Journal of Materials Research and Technology*, 8(2), 1933-1943. https://doi.org/10.1016/j.jmrt.2018.06.025

Lecomte-Nana, G., Bonnet, JP, & Soro, N. (2013). Influence of iron onto the structural reorganization process during the sintering of kaolins. *Journal of the European Ceramic Society*, 33(4), 661-668

Madejová, J. & Komadel, P. (2001). Baseline Studies of the Clay Minerals Society Source Clays: Infrared Methods. *Clays and Clay Minerals*, 49, 410-432.

Mache JR (2013). Mineralogy and physicochemical properties of smectites from Bana and Sabga (Cameroon). Use in the decolorization of a food vegetable oil. Doctoral thesis, University of Liège, Belgium, 145 p.

Maman MA, A. Rabani, F. Habbachi, F. Menai, A. Abdoulaye, and A. M'nif (2017). Characterization of two clay minerals of the Niger River Valley: Téra and Boubon. *Journal of the Tunisian Chemical Society*, 19, 52-58.

Méité, N., Konan, LK, Tognonvi, MT, Doubi, BIHG, Gomina, M., & Oyetola, S. (2021). Properties of hydric and biodegradability of cassava starch-based bioplastics reinforced with thermally modified kaolin. *Carbohydrate Polymers*, 254, 117322. https://doi.org/10.1016/j.carbpol.2020.117322

Msinjili, NS, Gluth, GJG, Sturm, P., Vogler, N., & Kühne, H.-C. (2019). Comparison of calcined illitic clays (brick clays) and low-grade kaolinitic clays as supplementary cementitious materials. *Materials and Structures*, 52(5), 94. https://doi.org/10.1617/s11527-019-1393-2

Mulewa, W., Tahir, M., & Amin, NAS (2017). MMT-supported Ni/TiO2 nanocomposite for low temperature ethanol steam reforming toward hydrogen production. *Chemical Engineering Journal*, 326, 956-969. https://doi.org/10.1016/j.cej.2017.06.012

N'guettia, RK, Aboua, NK, Diarra, M., Kpan Kpan, GK, Soro, BD, Meite, L., Gombert, B., Dembele, A., & Traore, KS (2019). Study of the influence of operating parameters on the removal of ciprofloxacin by clay-based materials. *International Journal of Biological and Chemical Sciences*, 13(1), 543-556. https://doi.org/10.4314/ijbcs.v13i1.42

N'Guettia, K.R., Diarra, M., Soro, B.D., Aboua, K.N., et al. (2023). Degradation of chlorantraniliprole by photocatalysis of supported titanium dioxide: Effect of operating parameters. African *Journal of Environmental Science and Technology*, 17(9), 209-218. https://doi.org/10.5897/AJEST2022.3157

Nwosu, F.O., Ajala, O.J., Owoyemi, R.M., & Raheem, B.G. (2018). Preparation and characterization of adsorbents derived from bentonite and kaolin clays. *Applied Water Science*, 8(7), 195. https://doi.org/10.1007/s13201-018-0827-2

Ségnéninhinténin Bakary Soro, Mariame Coulibaly, Legré Paul Gauly, Seiny Roger N'Dri, Ali Sanou & Albert Trokourey (2023). Characterization of Clay Materials from Côte d'Ivoire: Possible Application for the Electrochemical Analysis. *Journal of Materials Science Research*; 12, No. 1, 51-64.

Soro, BD, N'guettia, RK, Diarra, M., Aboua, NK, Meite, L., N'zue, YJV, Mamadou, K., & Traoré, SK (2023). Adsorption of a basic dye on a fixed-bed column of clay beads. *International Journal of Innovation and Applied Studies*, 41(1) pp. 79-87

Shahid, M., McDonagh, A., Kim, JH, & Shon, HK (2015). Magnetized titanium dioxide (TiO2) for water purification: Preparation, characterization and application. *Desalination and Water Treatment*, 54(4-5), 979-1002. https://doi.org/10.1080/19443994.2014.911119

Sraw, A., Kaur, T., Pandey, Y., Sobti, A., Wanchoo, RK, & Toor, AP (2018). Fixed bed recirculation type photocatalytic reactor with TiO2 immobilized clay beads for the degradation of pesticide polluted water. *Journal of environmental chemical engineering*, 6(6), 7035-7043.

Touré, GA, & Kouassi, KS (2017). Kapélé ceramics (Korhogo – northern Ivory Coast): On the intervention of men in a feminine art. *Gabonese Review of History and Archaeology*, e No. 2 pp. 14-27

Soro D., Bakayoko S., D. Dao, T. Bi Tra, P. Angui and O. Girardin (2011). Soil fertility diagnosis in the North-Central part of Côte d'Ivoire. *African Agronomy*, 23 (3), 205 - 215

Sei, J., Touré, AA, OlivierFourcade, J., Quiquampoix, H., Staunton, S., Jumas, JC and Womes, M. (2004). Characterization of kaolinitic clays from Côte d'Ivoire (West Africa). *Applied Clay Science*, 27(34), 235-239.

Rabani Adamou, Maimouna Soumaïla, Adamou Zanguina, Maman Maazou, Moussa Harouna, Moussa Konaté, Alassane Abdoulaye (2013). Use of clay materials from Niger in the decontamination of water contaminated by pyrethroid insecticides. Annals of Abdou Moumouni University, Volume XV-A, pp. 1426

Rouquerol, F., Rouquerol, J., & Sing, K. (1999). CHAPTER 2—Thermodynamics of Adsorption at the Gas–Solid Interface. In F. Rouquerol, J. Rouquerol, & K. Sing (Eds.), Adsorption by Powders and Porous Solids (pp. 27-50). *Academic Press*. https://doi.org/10.1016/B978-012598920-6/50003-8

Said, M., Erlangga, N., Alfarado, D., Suheryanto, S., & Nurnawati, E. (2023). Adsorption and Photocatalytic Activity of Bentonite–Titanium Dioxide on the Degradation of Methylene Blue Dyes. Indonesian *Journal of Fundamental and Applied Chemistry*, 126-132 . https://doi.org/10.2139/ssrn.4462431

Ségalen, P. (1969). Contribution to the knowledge of the color of sesquioxide soils of the intertropical zone: yellow soils and red soils. *Cah. ORSTOM. ser. Pédol*., vol. VII, no. 2, 1969.

Sun, Q., Zhang, W., Qian, H. (2016). Effects of high temperature thermal treatment on the physical properties of clay. *Environmental Earth Sciences*, 75(7), 610. https://doi.org/10.1007/s12665-016-5402-2

Volzone C., J. Ortiga (2006). Removal of gases by thermal-acid leaked kaolinitic clays: Influence of mineralogical composition. *Applied Clay Science*, 32, 87–93.

Wang, Y., Lin, X., Wen, K., Zhu, J., & He, H. (2014). Effects of organic templates on the structural properties of porous clay heterostructures: A non-micellar template model for porous structure. *Journal of Porous Materials*, 22(1), 219-228. https://doi.org/10.1007/s10934-014-9888-2

Yang S, Liang G, Gu A, Mao H (2013). Synthesis of TiO_2 pillared montmorillonite with ordered interlayer mesoporous structure and high photocatalytic activity by anintra-gallery templating method. *Mater. Res. Bull.*, 48, 3948–3954.

Zaaboul F., Canle M., Haoufazane C., Santaballa J. A., et al. (2024) A. Sunlight-Driven Photodegradation of RB49 Dye Using TiO2-P25 and TiO2-UV100: Performance Comparison. Coatings. 2024; 14(10):1270. https://doi.org/10.3390/coatings14101270

Zaki O., Abdoulaye A., DL Nomao, P. Rumori, GT Palomino, I. Amadou (2008). Characterization of Soils of Irrigated Perimeters of Western Niger by X-Ray Diffraction", *J Soc Ouest-Afr Chim*, vol. 26, pp. 89–97